AIP | Review of Scientific Instruments

Combined frequency modulated atomic force microscopy and scanning tunneling microscopy detection for multi-tip scanning probe microscopy applications

Ireneusz Morawski, Richard Spiegelberg, Stefan Korte, and Bert Voigtländer

Citation: Review of Scientific Instruments **86**, 123703 (2015); doi: 10.1063/1.4936975
View online: http://dx.doi.org/10.1063/1.4936975
View Table of Contents: http://scitation.aip.org/content/aip/journal/rsi/86/12?ver=pdfcov
Published by the AIP Publishing

Combined frequency modulated atomic force microscopy and scanning tunneling microscopy detection for multi-tip scanning probe microscopy applications

Ireneusz Morawski,[1,2] Richard Spiegelberg,[1] Stefan Korte,[1] and Bert Voigtländer[1]
[1]*Peter Grünberg Institut (PGI-3) and JARA-Fundamentals of Future Information Technology, Forschungszentrum Jülich, 52425 Jülich, Germany*
[2]*Institute of Experimental Physics, University of Wrocław, pl. M. Borna 9, 50-204 Wrocław, Poland*

(Received 5 August 2015; accepted 19 November 2015; published online 15 December 2015)

A method which allows scanning tunneling microscopy (STM) tip biasing independent of the sample bias during frequency modulated atomic force microscopy (AFM) operation is presented. The AFM sensor is supplied by an electronic circuit combining both a frequency shift signal and a tunneling current signal by means of an inductive coupling. This solution enables a control of the tip potential independent of the sample potential. Individual tip biasing is specifically important in order to implement multi-tip STM/AFM applications. An extensional quartz sensor (needle sensor) with a conductive tip is applied to record simultaneously topography and conductivity of the sample. The high resonance frequency of the needle sensor (1 MHz) allows scanning of a large area of the surface being investigated in a reasonably short time. A recipe for the amplitude calibration which is based only on the frequency shift signal and does not require the tip being in contact is presented. Additionally, we show spectral measurements of the mechanical vibration noise of the scanning system used in the investigations. © *2015 AIP Publishing LLC.* [http://dx.doi.org/10.1063/1.4936975]

INTRODUCTION

Measurements of the conductivity and the local potential of nanostructures are of great interest.[1–4] In order to yield comprehensive information about conductivity of 3D down to 1D nanostructures, four probe measurements are required to get rid of contact resistances. Besides charge transport measurements via lithographically structured contacts, multi-tip scanning tunneling microscopy (STM) has also been recently used to study charge transport in nanoelectronic devices.[5–8] As nanoelectronic devices consist of (semi) conducting parts as well as insulating parts, the use of frequency modulated atomic force microscopy (FM-AFM)[9] combined with STM[10] is desirable in order to access these both parts of the investigated sample. AFM provides topography information independent of the resistivity of the observed structures, while STM fulfills the demand of the conductivity measurements, down to the atomic scale.

The topography signal requires a bandwidth on the order of kHz in order to acquire a topography image of the micrometer scale in a reasonable time. The resonance frequency of the quartz resonator used as a FM-AFM probe plays a crucial role in the limitation of the bandwidth. Additionally, a small, compact, and multi-tip measurement instrument, where all tips are positioned independently in the sub-micrometer scale, requires micrometer lateral sizes of the quartz resonator. Among few types of quartzes[11] accessible in the market, the needle-sensor[12–14] satisfies these needs completely. Its eigenfrequency can be chosen from 640 kHz to 2 MHz, while its footprint is in tens of the micrometer range only.[15,16] This quartz resonator as the FM-AFM probe is both electrically excited and its mechanical oscillations are electrically detected simplifying mechanical construction and wiring of the AFM scanner. This becomes a great advantage when the multi-tip scanning probe microscopy (SPM) is required.

The last requirement which is met in four-tip conductivity measurements concerns independency of potential setting onto each tip with respect to the sample potential. In common applications, the potential of the tip with respect to the sample is simply created by the bias voltage applied to the sample, while the tip is on the virtual ground of the input amplifier. In the case of the four-tip measurements, such a solution cannot be used, because each tip has to be biased independent of the other tips. The known and utilized solution is mounting an electrically isolated tip on the quartz resonator, which is done for a qPlus sensor[17] and a needle sensor as well.[18] Nevertheless, such a circuit increases the number of required electric pins from 2 up to 3, and in the case of the multi-tip construction, it increases the complexity of the wiring, e.g., shielding, feed-throughs. In order to avoid this problem, an inductive coupling of the frequency shift and the tunneling current is presented and considered in this paper showing its utility in fast scanning of a complex sample. Similar to the topography image, the tunneling current through conductive parts of the sample can be imaged simultaneously. This imaging mode is analogues to conductive atomic force microscopy.[19]

In addition, we present a method for the oscillation amplitude calibration which can be performed by a free oscillating tip. Finally, the noise density of the scanning system is measured in the STM and AFM operation mode and then discussed.

ELECTRONIC SETUP

The tunneling current circuit and the frequency shift circuit are combined by means of a transformer, as shown in Fig. 1. The primary coil is driven by the output signal of the frequency demodulator (at around the resonance frequency of the sensor). The secondary coil provides the sinusoidal signal to the quartz and additionally allows for a flow of the current from the tip to the current-to-voltage (I/V) converter. The tunneling current is typically a low frequency signal with a bandwidth of a few kilohertz chiefly determined by the I/V converter, while the resonance frequency of the needle sensor quartz is above a few hundred kilohertz.[11,16] This means that both signals are separated in the frequency domain by about three orders of magnitude. This allows the utilization of just bandpass filters instead of more complex frequency detectors in order to electrically separate them. The I/V converter acts intrinsically as a low pass filter,[16,20] while the frequency demodulator circuit requires a high pass filter, when a modulation of the tip bias voltage is established. Measurements have shown that a second order passive filter with a cut-off frequency of about 200 kHz applied at the output of the FM preamplifier fulfills this requirement (Fig. 1). It is reported in Ref. 21 that the virtual ground is modulated by tunneling current oscillation at quartz frequency and this modulation can perturb detected oscillations from the quartz through the coupling capacity. In the presented circuit, the capacity between resonator electrodes plays this role, which equals about 0.5 pF[16] for a 1 MHz needle sensor. The mentioned virtual ground modulation arises from the relatively low slew rate of the used operational amplifier (here OPA111[22]). Nevertheless, this effect can be neglected due to much higher inner impedance of the virtual potential (non-inverting input of the opamp) than impedance of the FM preamplifier, both in the case of KolibriPreamp[23] or voltage preamplifier.[16]

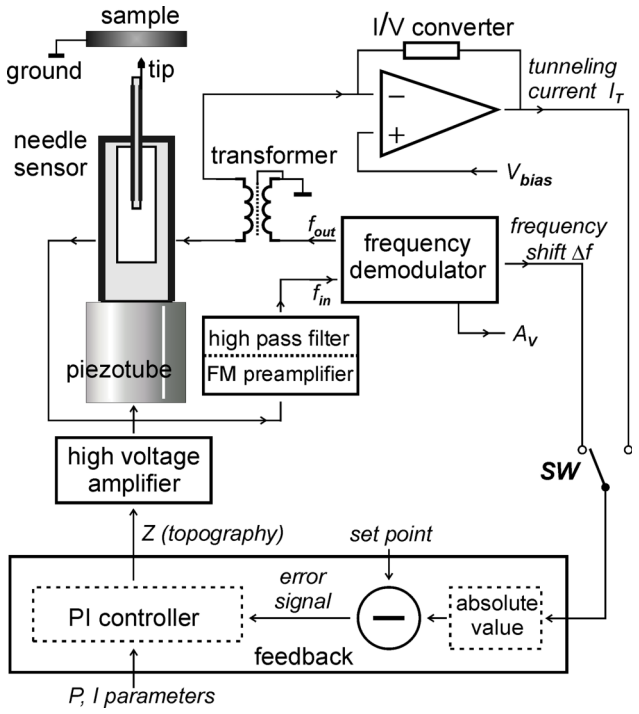

FIG. 1. Block diagram of the scanning probe microscopy, where the measured signals, frequency shift Δf, and tunneling current I_T are combined in one by means of inductive coupling (transformer). In this solution, the sample can be grounded (or put on a constant bias potential) independent of the tip bias voltage; only two wires are necessary to connect the probe, here a needle-sensor. The diagram shows additionally the z-signal feedback loop, while x-y movement is omitted. The switch SW connects either Δf or I_T to the feedback loop of the topography signal.

The transformer contains a grounded shield between its coils to avoid infiltration of interference with the highly sensitive I/V converter input from the primary coil. In general, the wiring of high impedance signals must be done with sufficient attention concerning shielding, grounding, and reducing of parasitic capacitance.[24,25] Therefore, a double shielded coaxial cable (triaxial cable) and an appropriate UHV feed-through were used to build a common branch from the secondary coil up to the probe.

The inductive coupling presented here enables the possibility to set the sample at a given potential independent of the tip bias voltages; in particular, the sample can be grounded. The potential of the tip with respect to the sample is set by the so-called voltage shifter[26] to a value which is delivered to the V_{bias} input. This allows constructing the multi-tip SPM with simultaneous recording of the tunneling current and frequency shift of all probes. Additionally, such a solution reduces the number of wires going to a probe sensor to the absolute minimum, i.e., two. This makes multi-tip SPM construction simpler and more compact.

The easyPLL device[27] has been used as a frequency demodulator in tracking mode[28] with a constant mechanical oscillation amplitude. In this mode, there are two feedback loops in order to maintain oscillations. One keeps mechanical amplitude constant independent of varying damping of the quartz oscillation giving information about this damping factor (dissipation output), and the other feedback channel follows (tracks) changes in resonance frequency, which are proportional to the tip-sample force gradient, by maintaining a constant phase of the sinusoidal signal (frequency shift Δf output).

APPLICATION

In Fig. 2, a large scale fast scanned image of the AFM topography, as well as a tunneling current image, is presented. A small piece of the logic part of an integrated circuit has been scanned in about 25 min (size 8 μm × 8 μm, 1024 × 1024 points). The investigated sample was polished in order to uncover the metallic pins. During the scanning process, the frequency shift was used as the z-feedback signal, while tunneling current was recorded as a free signal.[29] So, the AFM topography image (Fig. 2(a)) reflects approximately a surface of constant force gradient. In the tunneling current image (Fig. 2(b)), the grey background reflects the nonconductive substrate, the current equals zero, and bright spots reveal conductive parts, here metallic pins.

Due to the polishing process, the nonconductive part of the sample is also locally scratched which is visible as darker lines and spots in the topography signal. The simultaneously recorded current image does not reveal such features, which is illustrated in Fig. 3, where height profiles along the red

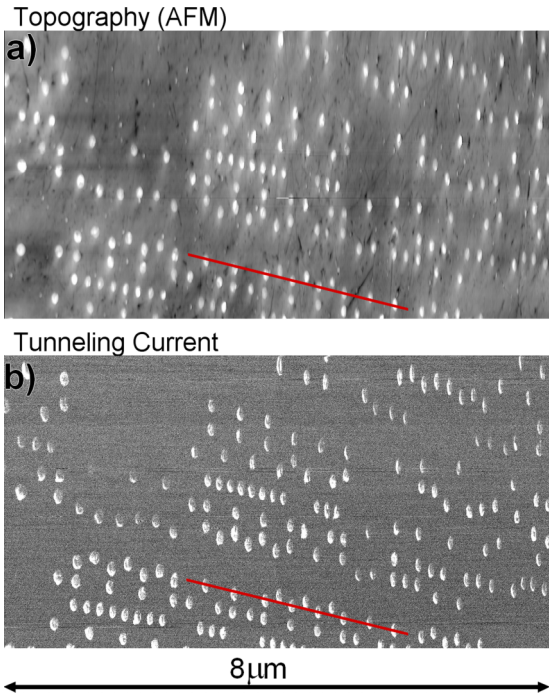

FIG. 2. Scan of the logic area of an integrated circuit. (a) AFM topography and (b) tunneling current images. Metallic pins are visible in both images (bright dots); however, additionally, some features located on the nonconductive substrate are visible only in the AFM topography scan. Scanning speed: about 6 μm/s, set point of the frequency shift: +30 Hz, frequency demodulator bandwidth: 400 Hz, tip bias voltage: −0.7 V, oscillation amplitude: 0.8 nm, height in topography: up to 10 nm, and recorded current: up to 20 pA.

lines in Fig. 2 are presented. It can be concluded that both signals are independent in the sense of the imaging process of the investigated surface. It has been noticed that a tunneling current spreading in the sample can modify the capacitive electrostatic force between the tip and the sample.[30] However, this does not apply to the present case, since this change is significant only on the semiconductor samples with relatively high resistivity in the order of Ω cm, and higher. In the case of the metallic pins (high conductance), the mentioned effect is negligible.

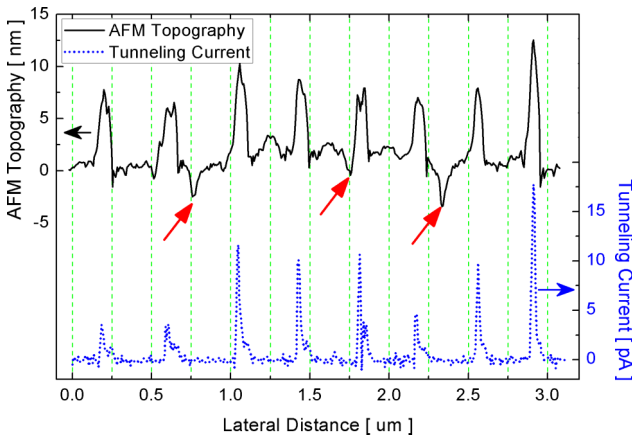

FIG. 3. Profiles along the red lines in Fig. 2. Apart from apparent pins, the AFM topography reveals dimples, marked by red arrows, which are not recorded in the current signal. The latter reveals only the metallic pins of the investigated sample.

The average height of the pins is about 5 nm (see Fig. 3), which is a large distance on the atomic scale; nevertheless, fast scanning was still possible at about 6 μm/s. This is due to the high resonance frequency of the needle sensor of 1 MHz. It means that the tip advances laterally along the surface about 6 pm per oscillation period, while, e.g., using tuning fork quartz,[31] this distance would be equal to about 180 pm at the scan speed mentioned above.

Detailed images of a single pin are shown in Fig. 4. Apart from the dimples mentioned above, a small piece of material is also present on the substrate, marked by a red arrow. This feature is not detected in the current signal, likewise, giving the simple conclusion that it is non-conductive material. As it is seen in Fig. 4(b), the tunneling current recorded from a metallic pin varies along a lateral distance; this can be due to contaminants on the sample surface which were not cleaned in the usual way under UHV conditions.

It is worth noticing that the bandwidth of the frequency demodulator was set to 400 Hz, which is not the maximum value accessible with the easyPLL device, namely, 1300 Hz. On the one hand, narrowed down bandwidth reduces maximum possible scan speed; on the other hand, the total noise increases with the bandwidth to the power of 1.5.[32] In the case of 400 Hz, the frequency shift noise is reduced almost 6 times in comparison with 1300 Hz, resulting in a more stable process of scanning. This shows that the bandwidth of the frequency demodulation is not the only crucial parameter in fast scanning of large areas.

AMPLITUDE CALIBRATION

The mechanical oscillation amplitude is an important quantity in FM-AFM and several methods have been proposed in order to determine this quantity.[17,29,33] The method described in the following is based on considerations reported in Ref. 34, however, applied for completely electrically detected deflection signals.

In order to estimate the amplitude A, the analysis of the spectral noise of the frequency shift signal is performed. It is known that this noise consists of three components, namely, detector, thermal, and oscillation noise, given by the following

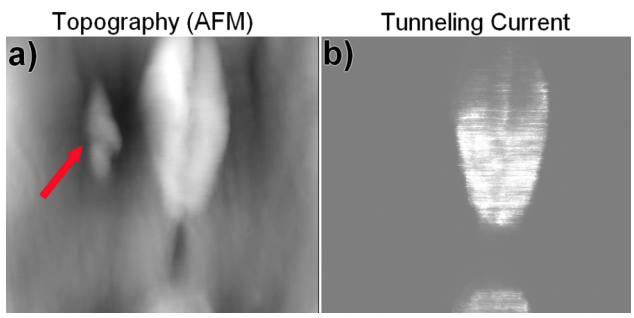

FIG. 4. Image of a single pin. (a) The AFM topography and (b) tunneling current. A nonconductive structure is visible in the AFM image, marked by a red arrow, while it is not recorded in the tunneling current. Scan area: 0.5 μm × 0.5 μm, scanning speed: 1 μm/s, set point: +9.5 Hz, frequency demodulator bandwidth: 400 Hz, the tip bias voltage: −1.0 V, oscillation amplitude: 0.8 nm, and tunneling current range: up to 10 pA.

terms:[35]

$$n_{detect}(f) = \sqrt{2} n_q \frac{1}{A} f, \tag{1}$$

$$n_{therm} = \sqrt{\frac{k_B T f_0}{\pi k Q}} \frac{1}{A}, \tag{2}$$

$$n_{osc} = \frac{n_q f_0}{\sqrt{2} Q} \frac{1}{A}. \tag{3}$$

Six physical quantities are involved in the calculation of these noise components, namely, temperature T, spring constant k, resonance frequency f_0, quality factor Q, mechanical oscillation amplitude A, and detector floor noise n_q. All terms depend on the reciprocal of the amplitude A. Additionally, the detector noise depends linearly on the modulation frequency f. These two facts enable the possibility to estimate two of the six quantities. The first four parameters mentioned above are relatively easy to determine; thus, amplitude and detector noise can be determined by means of fitting the simulated total noise to the experimentally measured noise spectrum.

The resultant spectral noise is described as follows:

$$n_{res}(f) = \sqrt{[n_{detect}(f)]^2 + [n_{therm}]^2 + [n_{osc}]^2}. \tag{4}$$

The experimental data can be fitted by a function with two parameters a and c,

$$n(f) = \sqrt{a f^2 + c}, \tag{5}$$

which are related to the amplitude A and the detector floor noise n_q as

$$\begin{cases} A = \sqrt{\dfrac{4 k_B T}{\pi k}} \dfrac{Q f_0}{4cQ^2 - a f_0^2}. \\ n_q = \sqrt{\dfrac{a}{2}} A \end{cases} \tag{6}$$

Finally, the amplitude coefficient C which relates the electrical readout voltage to the mechanical amplitude is given by

$$C = \frac{A_V}{A} \quad \left[\frac{V}{nm}\right]. \tag{7}$$

Experimental data of the frequency shift noise obtained from two readout amplitudes, 25 mV and 50 mV, are shown in Fig. 5, squares and triangles, respectively. Fitting of the theoretical data was performed for the following input quantities: T = 298 K (ambient temperature), k = 1.7 MN/m,[36] f_0 = 996 681 Hz, and Q = 15.4 k (two last obtained from the resonance curve); for these numbers, in particular this temperature, the oscillation noise contributes less than 2% to the constant noise component. Nevertheless, the fitting procedure includes the oscillation noise in order to provide Equation (6) to be accurate also for low temperatures or low Q-environments. The best fit, shown in Fig. 5 as solid lines, was simulated for the oscillation amplitudes 42 pm and 84 pm, at 25 mV and 50 mV of the readout amplitude, respectively, and a detector noise of n_q = 0.76 fm/√Hz. Hence, the amplitude coefficient C equals 0.595 V/nm. This value is in good agreement with the value obtained from a method relying on the measurement of the tunneling current proposed in Ref. 33, namely, 0.61 V/nm. The

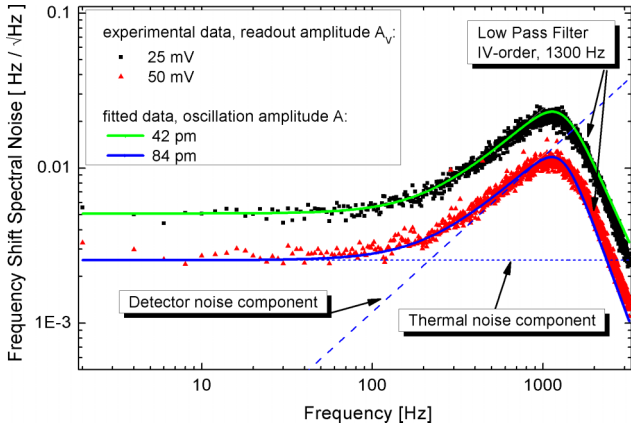

FIG. 5. Experimental determination of the amplitude coefficient C performed for two readout amplitudes A_V: 25 mV and 50 mV; theoretical simulations (blue and green lines) are fitted to the experimental data, lines and symbols, respectively, for a known readout amplitude A_V. The detector and thermal noise components are shown as a dashed line and a dotted line, respectively; the former depends linearly on frequency, while the latter is constant as a function of frequency, enabling the determination of the oscillation amplitude as well as the detector noise n_q. The number of averaging of the shown data equals to 30.

coefficient can also be calculated from sensor and preamplifier sensitivity,[36] which results in a value of 0.63 V/nm.

However, this coefficient should not be treated as a fundamental value because it depends on (i) the amplification of the preamplifier and high pass filter (if applied), (ii) rectifier gain in the amplitude determination circuit scheme, (iii) damping in the cables, and (iv) sensitivity of the used quartz. Therefore, the amplitude calibration should be conducted whenever something is changed or replaced in the detector circuit. The amplitude calibration method presented here is a fast and efficient procedure which does not require tip-sample interaction.

In the last part of this Chapter, we derive the relative uncertainty of the amplitude from Eq. (6). The parameters a and c are obtained from the fitting procedure and their uncertainties u_a and u_c as well. Therefore, both numbers are correlated and the relative combined uncertainty[37] expressed from Eq. (6) is given by

$$\left(\frac{u'_A}{A}\right)^2 = \frac{1}{4}\left(\frac{4Q^2 u_c + f_0^2 u_a}{4Q^2 c - f_0^2 a}\right)^2. \tag{8}$$

The Q and f_0 are obtained from the same measurement of the so-called resonance frequency curve; therefore, these two correlated quantities deliver next contribution as follows:

$$\left(\frac{u''_A}{A}\right)^2 = \frac{1}{4}\left\{\left[\frac{4cQ^2 + a f_0^2}{4cQ^2 - a f_0^2}\right]^2 \left(\frac{u_Q}{Q} + \frac{u_{f_0}}{f_0}\right)^2\right\}, \tag{9}$$

where u_Q and u_{f_0} are uncertainties of the Q factor and resonance frequency, respectively. The uncertainties of the remaining quantities, k and T, which can be treated as uncorrelated, contribute to u_A in the following way:[37]

$$\left(\frac{u'''_A}{A}\right)^2 = \frac{1}{4}\left\{\left(\frac{u_k}{k}\right)^2 + \left(\frac{u_T}{T}\right)^2\right\}, \tag{10}$$

where u_k and u_T are uncertainties of respective quantities.

Thus, final relative uncertainty of amplitude determination taking into account the three mentioned above contributions is given by

$$\frac{u_A}{A} = \frac{1}{2}\sqrt{\left(\frac{\pi A^2 k}{4k_B T f_0 Q}\right)^2 \left(4Q^2 u_c + f_0^2 u_a\right)^2 + \left[1 + \frac{\pi n_q^2 f_0 k}{k_B T Q}\right]^2 \left(\frac{u_Q}{Q} + \frac{u_{f_0}}{f_0}\right)^2 + \left(\frac{u_k}{k}\right)^2 + \left(\frac{u_T}{T}\right)^2}, \quad (11)$$

where the terms in the denominator in Eq. (8) and in square brackets in Eq. (9) were expressed into physical quantities using Eqs. (1)–(3) and (5). The first term in Eq. (11) has been reaching about 0.5% for the spectral noise, shown in Fig. 5, acquired by a spectrum analyzer.[38] This means that the amplitude can be determined with an accuracy of about 1 pm by means of the described fitting procedure. It is worth mentioning that the term in the square brackets for a high enough Q factor and low enough detector floor noise n_q is close to 1; therefore, the amplitude uncertainty is mainly determined by the highest relative uncertainty of k, T, Q, or f_0.

SCANNING SYSTEM NOISE

In this section, the tunneling current noise and the frequency shift noise are used in order to deduce information on the mechanical vibrations of the scanning system. There are two main reasons for noise: thermal vibrations and resonances. In general, the former have continuous spectral density, and the latter have a discrete spectrum. Both occur as mechanical noise or electronic noise in the system. However, in the case of complex systems, usually no more than two noise sources play a major role. It stems from the summation rule of energy carried by these components, i.e., the resultant value of a given measured signal is the square root of the sum of the squares of particular noises. In practice, a noise contribution with a magnitude of less than 50% of the reference level can be neglected, because its contribution to the total noise is lower than 10%. Additionally, the magnitude of various noises can differ several orders in a given system.

The intrinsic noise of the scanning system (SPM scanner) was investigated using the STM/AFM probe being in contact mode. Theoretically, when the tip-sample distance is small enough, the noise of the tunneling current or the force gradient is related to mechanical oscillations of the scanning system. In other words, in such a case, the probe acts as a mechanical noise detector. On the other hand, due to drift effects, it is impossible to maintain a constant tip-sample distance for a sufficient time, which is required to conduct appropriate measurements. Therefore, the distance is stabilized using the z-feedback loop but with a long response time of the proportional-integral (PI) controller.[39] This ensures that all signal components with frequencies above the reciprocal of the response time are transmitted through the PI controller and do not influence the tip-sample distance. In our experiment, the PI time constant was set to about 100 s, which is long enough to record intrinsic SPM scanner noise from 1 Hz. Finally, knowing the functional dependence of the recorded signal with respect to the tip-sample distance, one can directly estimate equivalent mechanical noise for a given system.

In the case of the tunneling current, such a dependence is well known and established as an exponential function,[10] while frequency shift dependence is rather not described by an analytical function.[40,41] However, the measurements performed for the investigated system and sample have shown that the frequency shift can also be described as an exponential function for a quite wide range of tip-sample distance, as shown in Fig. 6. In this figure, both dependencies are presented in a log scale revealing their exponential character within a certain range of tip-sample distance. Starting from the exponential dependence of the signal,

$$S(z) \propto e^{(\kappa z)}, \quad (12)$$

and differentiating it,

$$\delta S = \kappa S(z)\, \delta z, \quad (13)$$

one gets the following term for equivalent mechanical noise along the z coordinate:

$$\delta z = \frac{\delta S}{\kappa S(z)}, \quad (14)$$

where κ denotes the slope coefficient of the linear fit, and δS denotes the total noise measured for a given signal S, here tunneling current or frequency shift, at a given z position, which is determined by the set point $S(z)$ and maintained at this equilibrium position by the slow feedback loop.

Measurements were performed at a few chosen set points: three for tunneling current and two for the frequency shift. The results are presented in Table I. The calculations include

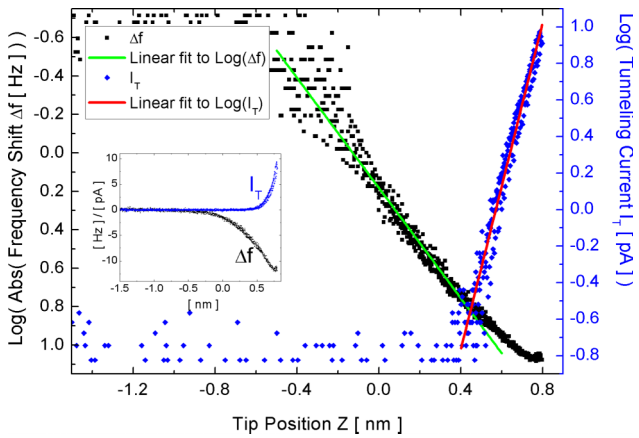

FIG. 6. Dependence of the frequency shift and a tunneling current recorded simultaneously, black and blue dots, shown in log scale versus tip position (inset: in linear scale). The exponential part of both signals is approximated by a linear function in log scale, green and red lines, respectively. The noise analysis was performed within these exponential ranges.

TABLE I. Equivalent z-noise of the scanning system obtained from detection of tunneling current noise and frequency shift noise at a slow response of the z-feedback loop.

Set point I_T	Measured noise $\delta(I_T)$	Position z-noise δz	Detector inner noise
8.0 pA	2.65 pA-rms	16.6 pm-rms	0.15 pA-rms
18.0 pA	3.86 pA-rms	10.7 pm rms	
39 pA	8.44 pA-rms	10.8 pm-rms	
Δf	$\delta(\Delta f)$	δz	
−5.9 Hz	0.20 Hz-rms	12 pm-rms	0.05 Hz-rms
−7.3 Hz	0.23 Hz-rms	10 pm-rms	

intrinsic noise of the detector δS_0 in the following way:

$$\delta S = \sqrt{\delta^2 S_m - \delta^2 S_0}, \quad (15)$$

where δS_m is the noise recorded in contact, and δS_0 is the detector noise, i.e., recorded when the tip is out of contact. The latter is shown in the last column. Values δz obtained from tunneling current and frequency shift are in agreement, which means that the results are independent of the detector type. The noise of the high voltage z-amplifier (see Fig. 1) was equal to about 0.1 mV-rms; this value is transferred to z-noise through piezo-constant, 5.6 nm/V, and leads to a component equals to about 0.6 pm-rms, which can be neglected. It is obvious that the considered z-noise equivalent value includes also mechanical vibrations in x and y directions. Nevertheless, the measured signal dependence is rather strongly dependent on the z-coordinate than on x-y; otherwise, significant changes of the signal would be observed that are caused by thermal lateral drift of the tip-sample system.

Values of the total noise presented so far do not deliver information about the character and the origin of the mechanical noise. Therefore, simultaneously with measurements of the total values, a spectral analysis of the noise was performed as well. The results are presented in Figs. 7 and 8, for the tunneling current and the frequency shift, respectively.

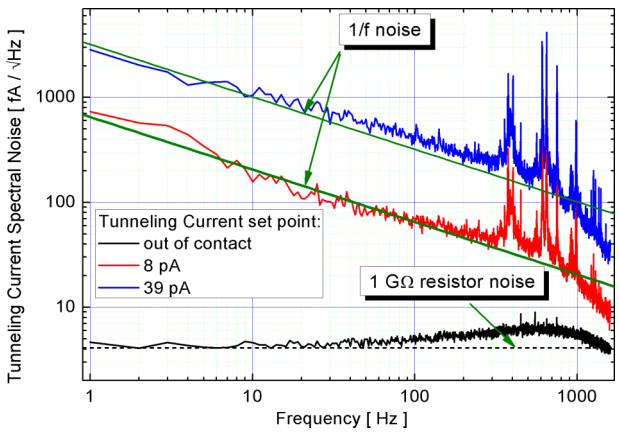

FIG. 7. Spectral noise of the tunneling current recorded for: tip out of contact (black line) and chosen set points in contact mode (red and blue lines). The latter include square root subtraction of the free tip noise, Eq. (15). In the case of the tip in contact, a 1/f dependence is readily noted. It is most likely that the peaks at higher frequencies arise from mechanical excitation of the parts of the sample holder.

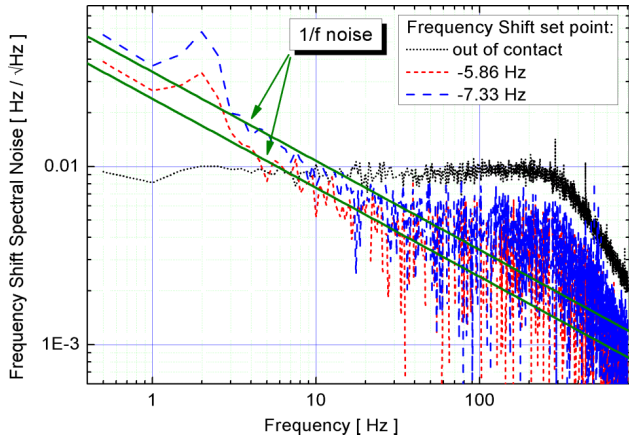

FIG. 8. Spectral noise of the frequency shift. Again, the 1/f noise is observed. The 2 Hz peak comes from resonance frequency of the spring suspension system.

Interestingly, the spectral noise reveals 1/f dependence of the mechanical vibrations for both cases. The same dependence was observed for tunneling current and reported in Ref. 42. It is known that such a kind of noise is the effect of the stochastic behavior of nature,[43,44] including striving to the thermal equilibrium of the considered system. Detailed research of the so-called floor noise performed for other reasons in FZJ laboratories reveals also 1/f dependence (Ref. 28, Figs. 3.22 and 3.23). It is most likely that this floor noise is transferred through the SPM damping systems and observed in present results. In such a case, about a 10^8 factor of suppressing can be estimated. Nevertheless, independent of the source of the observed system noise, the nature of the 1/f noise stays the same. The figures show also another conclusion, namely, that in the case of the tunneling current, the equivalent z-noise dominates over the detector noise even for small set points, while in the case of the frequency shift, only a minor part for low frequency is above the frequency shift noise obtained from the "free" tip oscillations. The border frequency, here about 10 Hz, is far lower than the expected bandwidth, at least 1 kHz; therefore, the intrinsic vibrations observed in the scanning system play a minor role in comparison with the recorded frequency shift noise. With an increased oscillation amplitude, frequency shift noise can even be lowered.

CONCLUSIONS

The inductive coupling makes it possible to control the potentials of the tip and the sample independently, which straightforwardly leads to an application in the multi-tip SPM construction in order to perform, i.e., four-tip conductivity measurements. FM-AFM combined with STM enables investigation of conductive parts situated on a non-conductive substrate. Fast acquisition of the topography signal is possible due to a high resonance frequency of the applied needle sensor.

The presented amplitude calibration provides value with relatively high accuracy, <1%. It does not require the tip being in contact, which makes it easy and fast to apply. The spectral noise measurements of the mechanical vibration in the used

scanning system reveal 1/f noise, which is the fundamental type of noise met in the environment.

ACKNOWLEDGMENTS

This project was supported by a JARA-Start grant. The authors are indebted to Dr. Josef Mysliveček for design and implementation the voltage shifter which was applied as a part of the presented electronics.

[1]I. Matsuda, M. Ueno, T. Hirahara, R. Hobara, H. Morikowa, C. Liu, and S. Hasegawa, Phys. Rev. Lett. **93**, 236801 (2004).
[2]C. M. Polley, W. R. Clarke, J. A. Miwa, M. Y. Simmons, and J. W. Wells, Appl. Phys. Lett. **101**, 262105 (2012).
[3]C. Durand, P. Capiod, M. Berthe, J. P. Nys, Ch. Krzeminski, D. Stiévenard, Ch. Delerue, and B. Grandiddier, Nano Lett. **14**, 5636 (2014).
[4]T. Trenkler, P. De Wolf, W. Vandervorst, and L. Hellemans, J. Vac. Sci. Technol., B **16**, 367 (1998).
[5]J. Baringhaus, M. Ruan, F. Edler *et al.*, Nature **506**, 349 (2014).
[6]V. Cherepanov, E. Zubkov, H. Junker, S. Korte, M. Blab, P. Coenen, and B. Voigtländer, Rev. Sci. Instrum. **83**, 033707 (2012).
[7]O. Guise, H. Marbach, J. T. Yates *et al.*, Rev. sci. instrum. **76**, 045107 (2005).
[8]A. Bannani, C. A. Bobisch, and R. Moeller, Rev. Sci. Instrum. **79**, 083704 (2008).
[9]R. García and R. Perez, Surf. Sci. Rep. **47**, 197 (2002).
[10]C. J. Chen, *Introduction to Scanning Tunneling Microscopy* (Oxford University Press, New York, 2008).
[11]See www.statek.com for data from STATEK Corporation, USA.
[12]K. Bartzke, T. Antrack, K. H. Schmidt, E. Dammann, and Ch. Schatterny, Int. J. optoelectron. **8**, 669 (1993).
[13]U. Grunewald, K. Bartzke, and A. Antrack, Thin Solid Films **264**, 169 (1995).
[14]T. An, T. Nishio, T. Eguchi, M. Ono, A. Nomura, K. Akiyama, and Y. Hasegawa, Rev. Sci. Instrum. **79**, 033703 (2008).
[15]S. Heike and T. Hashizume, Jpn. J. Appl. Phys. **45**, 1996 (2006).
[16]I. Morawski, J. Blicharski, and B. Voigtländer, Rev. Sci. Instrum. **82**, 063701 (2011).
[17]F. J. Giessibl, Appl. Phys. Lett. **76**, 1470 (2000).
[18]S. Torbrügge, O. Schaff, and J. Rychen, J. Vac. Sci. Technol., B **28**, C4E12 (2010).
[19]A. Olbrich, B. Ebersberger, and C. Boit, Appl. Phys. Lett. **73**, 3114 (1998).
[20]P. R. Gray, P. J. Hurst, S. H. Lewis, and R. G. Meyer, *Analysis and Design of Analog Integrated Circuits*, 4th ed. (Wiley, New York, 2001).
[21]Z. Majzik, M. Setvin, A. Bettac, A. Feltz, V. Chab, and P. Jelinek, Beilstein J. Nanotechnol. **3**, 249 (2012).
[22]See www.ti.com for Burr-Brown Products, Texas Instruments, USA.
[23]See www.specs.com for SPECS Surface Nano Analysis GmbH.
[24]H. W. Ott, *Noise Reduction Techniques in Electronic Systems* (Wiley, New York, 1976).
[25]C. D. Motchenbacher and J. A. Connelly, *Low-Noise Electronic System Design* (Wiley-Interscience, New York, 1993).
[26]R. Hobara, N. Nagamura, S. Hasegawa, I. Matsuda, Y. Yamamoto, Y. Miyatake, and T. Nagamura, Rev. Sci. Instrum. **78**, 053705 (2007).
[27]See www.nanosurf.com for Nanosurf AG, Switzerland.
[28]B. Voigtländer, *Scanning Probe Microscopy: Atomic Force Microscopy and Scanning Tunneling Microscopy* (Springer, New York, Berlin, Heidelberg, 2015).
[29]I. Morawski and B. Voigtländer, Rev. Sci. Instrum. **81**, 033703 (2010).
[30]A. J. Weymouth, T. Wutscher, J. Welker, T. Hofmann, and F. J. Giessibl, Phys. Rev. Lett. **106**, 226801 (2011).
[31]F. J. Giessibl, Appl. Phys. Lett. **73**, 3956 (1998).
[32]Y. Hasegawa, T. Eguchi, T. An, M. Ono, K. Akiyama, and T. Sakurai, Jpn. J. Appl. Phys. **43**, L303 (2004).
[33]G. H. Simon, M. Heyde, and H.-P. Rust, Nanotechnology **18**, 255503 (2007).
[34]J. Lübbe, M. Temmen, S. Rode, P. Rahe, A. Kühnle, and M. Reichling, Beilstein J. Nanotechnol. **4**, 32 (2013).
[35]K. Kobayashi, H. Yamada, and K. Matsushige, Rev. Sci. Instrum. **80**, 043708 (2009).
[36]F. J. Giessibl, F. Pielmeier, T. Eguchi, T. An, and Y. Hasegawa, Phys. Rev. B **84**, 125409 (2011).
[37]Joint Committee for Guides in Metrology, in *Evaluation of Measurement Data—Guide to the Expression of Uncertainty in Measurement* (JCGM, 2008), Vol. 100, Chap. 5.
[38]From Hewlett Packard, model HP35670A.
[39]H. L. Wade, *Basic and Advanced Regulatory Control: System Design and Application*, 2nd ed. (ISA, Research Triangle Park, 2004).
[40]F. J. Giessibl, Phys. Rev. B **56**, 16010 (1997).
[41]U. Dürig, Appl. Phys. Lett. **75**, 433 (1999).
[42]R. Möller, A. Esslinger, and B. Koslowski, Appl. Phys. Lett. **55**, 2360 (1989).
[43]G. Vasilescu, *Electronic Noise and Interfering Signals* (Springer-Verlag, Berlin, Heidelberg, 2005).
[44]Sh. Kogan, *Electronic Noise and Fluctuations in Solids* (Cambridge University Press, 1996).